

Saturn Ring Data Analysis and Thermal Modeling

Coleman Dobson

Mentors: Linda Spilker, Estelle Deau

CIRS, VIMS, UVIS and ISS, (Cassini's Composite Infrared Spectrometer, Visual and Infrared Mapping Spectrometer, Ultra Violet Imaging spectrometer and Imaging Science Subsystem, respectively), have each operated in a multidimensional observation space and have acquired scans of the lit and unlit rings at multiple phase angles. To better understand physical and dynamical ring particle parametric dependence, we co-register profiles from these three instruments, taken at a wide range of wavelengths, from ultraviolet through the thermal infrared, to associate changes in ring particle temperature with changes in observed brightness, specifically with albedos inferred by ISS, UVIS and VIMS. We work in a parameter space where the solar elevation range is constrained to 12° - 14° and the chosen radial region is the B3 region of the B ring; this region is the most optically thick region in Saturn's rings. From this compilation of multiple wavelength data, we construct and fit phase curves and color ratios using independent dynamical thermal models for ring structure and overplot Saturn, Saturn ring, and Solar spectra. Analysis of phase curve construction and color ratios reveals thermal emission to fall within the extrema of the ISS bandwidth and a geometrical dependence of reddening on phase angle, respectively. Analysis of spectra reveals Cassini CIRS Saturn spectra dominate Cassini CIRS B3 Ring Spectra from 10 to 1000 microns, while Earth-based B Ring Spectrum dominates Earth-based Saturn Spectrum from 0.4 to 4 microns. From our fits we test our dynamical thermal models; from the phase curves we derive ring albedos and non-lambertian properties of the ring particle surfaces; and from the color ratios we examine multiple scattering within the regolith of ring particles.

Introduction

Cassini's Composite Infrared spectrometer, (CIRS), a dual Michelson interferometer, has acquired seven years worth of thermal data on Saturn's lit and unlit rings over a variety of ring geometries, which include solar phase angle, spacecraft elevation, local hour angle, and a range of solar elevation angles which span from 24° through ring equinox (0°). Understanding of the microstructure and microphysics of the rings has evolved from rings filled with individual particles in uniform distribution to bimodally divided A and B rings containing particles which clump into transient structures of characteristic sizes and orientations, self-gravity wakes, and viscous overstability. Important ring particle puzzles include: the effect of particle compaction on the visible, near-IR and thermal radiation from the rings; the vertical organization of ring particles (multilayer or monolayer), and the effect of particle compaction on this structure; correlating ring particle thermal conductivity with frosty regolith and/or porous particle aggregates; and the variance of ring thermal inertia with albedo, surface roughness and particle (or clump) spin.

Saturn's rings represent a medium within which ring particles have their temperatures determined by absorbed, conducted and emitted energy, and where the energy source functions depend upon the ring structure. Energy sources include direct, reflected and scattered solar input, mutual heating by neighboring ring particles, and thermal and visible radiation from Saturn. Because of mutual shading and heating between particles, thermal emission is determined not only by the physical properties of the ring particles, but also by the structural and dynamical properties of the ring itself. Individual particle properties include size, regolith characteristics, bond albedo, thermal emissivity and inertia, spin rate, and spin axis orientation. Ring structural and dynamical properties include optical depth, vertical thickness and particle size distribution. To model and understand ring thermal properties requires a significant amount of analysis; an analysis which will increase our knowledge of processes in planetary rings and with which we can compare to analogous processes in the early solar nebula to plausibly explain planetary and satellite origins.

Problem

To investigate and constrain physical and dynamical ring particle properties, we will perform the following three tasks: First, we will generate brightness and color profiles for the rings using ISS and VIMS data and compare the results at different wavelengths. From these profiles, we will create, model, and compare

thermal and optical phase curves for the B3 region of the B ring and fit existing models to data. Secondly, we will construct color ratios and normalized color ratios and compare results with literature. Thirdly, we will superpose Saturn, Solar, and Saturn ring spectra, therein utilizing all four of Cassini's optical remote sensing devices. The end goal is to correct for Saturn shine and perform a fit with photometric models to therein obtain a well-constrained optical albedo.

Our research goals are the following:

We are to compare at different wavelengths thermal and optical phase curves for selected locations in the rings, therein producing both a compilation of the many independent results of the rings from ISS, VIMS, and CIRS data sets and a discussion of wavelength dependent features. By producing I/F and thermal phase curves we will investigate the role of volume filling factor on ring particle temperature and the nature and behavior of ring particles. And concomitantly, what is relatively unexplored, we shall further investigate the flatness of the B ring unlit thermal phase curves and local time curves.

Regarding part two of the research plan, which is a work in progress, while Dones has produced an albedo value from one single phase angle, and Dr. Morishima used albedo values from fitting four CIRS scans, our approach would be novel in that it covers all phase space and is independent of the coupled input parameters in Dr. Morishima's dynamical model. We will have therefore created a well-constrained value of albedo, with which we can determine the impact of albedo (and color) in modulating ring temperature.

Methods

Data Mining:

We first sorted and obtained 9 tri-joint ISS, CIRS, and VIMS data profiles, which fell within a solar elevation angle range of 12° to 14° and spanned a start and stop time of, what is an approximate, January 2006 to January 2008 (Figure 1). We limited our first profile to a small section of the parameter space after which we would expand in parametric range (Figure 2). Then we used NASA's Planetary Data Systems (PDS) Rings Node Data Search OPUS Tool to download all calibrated ISS data and used NAIF (the Navigation and Ancillary Information Facility) and SPICE (the information system aiding in interpreting scientific observations from our space-based instruments), to download Cassini's operational flight projects kernels to begin navigation and reprojection of the tri-joint data sets. Once data mining, calibration, renavigation, and the removal of Saturn shadow functions, were complete, we proceeded to construct radial, brightness, and color profiles, as well as, phase curves, color ratios, and spectra; each of which is discussed after a brief section on our working parameter space and on Cassini's instruments (for a brief review of our ring modeling, please see the appendix).

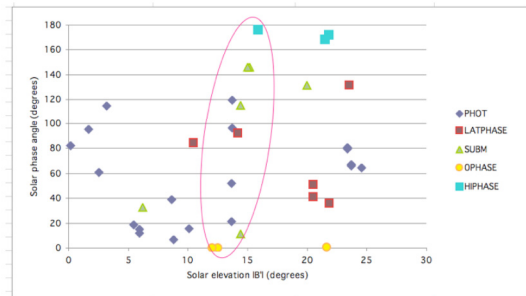


Figure 1. Selection of Joint Observations

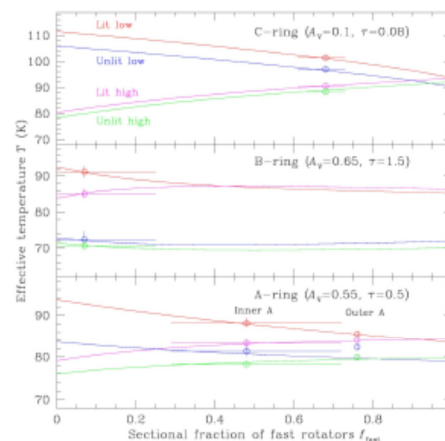


Figure 2. A Parametric Dependence

Parameter Space

The sufficiency in fulfilling our research proposal was in knowing the sensitivities of modeling parameters and choosing which to fix and which to vary. We are interested in three parameters, geometric albedo, local volume density, and thermal inertia, each of which is now further discussed.

Geometric Albedo

A value between 0 and 1, this is the ratio of actual brightness at zero phase to that of a Lambertian disk, respecting cross-section. That our CIRS and ISS phase curves display opposition effect shows the difficulty in determining this value; that is, reflectance is strongly peaked for a small range of near-zero phase angles. For albedo determination, we will use models of the rings' optical depth derived from VIMS and UVIS occultation results, which consider regional differences in phase functions.

Local volume density (filling factor) β

We use the characterization by N. Altobelli et al. (2007):

$$\beta = \beta_f \beta_c \varepsilon$$

where β_f is the fractional area of the fov by the emitters (the geometric filling factor);

β_c represents each spectrum resulting from a superposition of radiation from emitters at a distribution of temperatures; and ε is the infrared emissivities of the ensemble of emitters, where we are assuming that, to first order, we can separate these effects. Simply, β is factor scaling the radiance emitted by an ensemble of particles.

Investigation of the combined data sets will constrain the effect of local volume density (filling factor) of the rings upon comparing ISS and CIRS phase curves; specifically, the fall off behavior.

Thermal inertia

Thermal inertia is the square root of the product of the thermal conductivity, the physical density, and the heat capacity. This parameter quantifies the particles' heating and cooling rates via thermal emission as they move into and out from Saturn's shadow. We are interested in this region as around the shadow boundaries of the rings we see most drastic temperature changes. A low thermal inertia is inferred from the steepness of the cooling curves and implies a high porosity for regolith layers. As the cooling rate depends on the relation of particle spin period to thermal relaxation time, we see that deriving thermal inertia from our data sets requires specific dynamical thermal modeling.

In analyzing these phase curves, we can derive properties of the ring particle surface, which include surface roughness, surface porosity, and grain size. The effect of each on thermal inertia is non trivial and may help explain variations in thermal inertia as a function of ring radius.

Instruments

We wish to co-register data sets obtained from the following four optical remote sensing devices.

CIRS: Cassini's composite infrared spectrometer is a dual Michelson interferometer which measures thermal emission from wavelengths of 7 microns to 1 mm at an apodized spectral resolution programmable from 0.5 to 15.5 cm^{-1} . Focal Plane 1 (FP1), the far infrared interferometer, covers from 17 microns to 1mm and has a 0.25° fov, while FP3 and FP4, the mid infrared interferometer consists of two 1×10 arrays of 0.2 pixels which together span 7 to 17 microns (CDAP).

ISS : Cassini's Imaging Subsystem instrument consists of two cameras , a wide angle camera (WAC) with 3.5° fov and spectral range 380-1050nm, and a narrow angle camera (NAC) with fov 0.35° and spectral range 200-1050nm, both equipped with 1024×1024 CCDs. The cameras each have two filter wheels, with 12 filters on each wheel on the NAC and 9 filters on each wheel on the WAC (CDAP).

VIMS: Cassini's Visual and Infrared Mapping Spectrometer contains a pair of imaging grating spectrometers which measure reflected and emitted radiation from 0.35 to 5.2 microns and provide spectral images; more specifically, a full spectrum is obtained for every 0.03 pixel in arrays of up to 64×64 pixels. VIMS contains an infrared sensor channel covering from 0.85 to 5.2 microns and a visible sensor channel covering 0.35 to 1.05 microns, a coverage which together covers 95% of the integrated solar irradiance (CDAP).

UVIS: Cassini's Ultraviolet Imaging Spectrograph Subsystem contains: two spectrographic channels, the extreme ultraviolet channel (euV) and the far ultraviolet channel (fuV), which provide images and spectra covering the ranges from 56 to 118nm; a photometer channel used for stellar occultations by rings and atmospheres; a hydrogen-deuterium absorption cell channel which measures the relative abundance of deuterium and hydrogen from their Lyman- α emission; and an electronic and control subassembly.

Joint Phase Curves

To the question why focus on phase curves and not solar or optical depth curves, we answer as follows: We focus our analysis on phase curves because, to first order, variations in phase angle drive the largest

temperature changes on the lit face on the rings, with those of spacecraft elevation assuming a secondary effect. Specifically, using data from all four remote optical sensing devices, we can look at rings in different wavelengths and extract information regarding the nature of the ring particles (regolith, size distribution, lambertian...) from the shape of the phase curves. What is interesting is our comparison of two different operations: that of reflected versus emitted light.

As ISS, CIRS, and VIMS have obtained enough radial scans in enough parameter space, we conjectured to construct phase curves for the main rings using first our solar range of 12° to 14° and then our extended range; plots of Temperature or I/F versus phase angle. The only joint work previously investigated was done by Dones and Cuzzi, et. al.

Dones produced a radial single-scattering albedo with respect to 5 different filters (Figure 3), using only one single phase angle (left plot below). We intend to use all of phase space. And Cuzzi et al produced a joint I/F and Temperature curve (Figure 4).

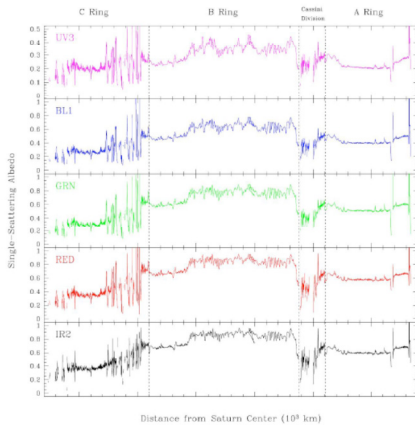


Figure 3. Dones Albedo Investigation

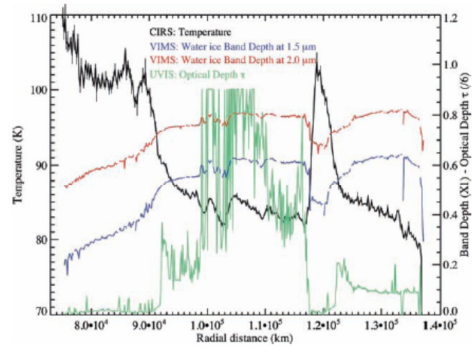


Figure 4. Cuzzi, et.al Multi-Plot

And, what is a further independent investigation, we have VIMS brightness profiles as a function of ring radius and VIMS color ratios (Figure 5). We intended to expand Cuzzi's method in the VIMS, ISS, and CIRS compilation.

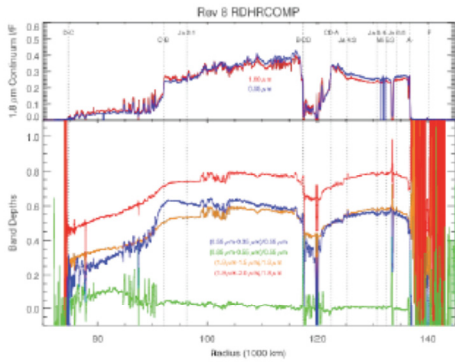


Figure 5. VIMS Brightness Profile

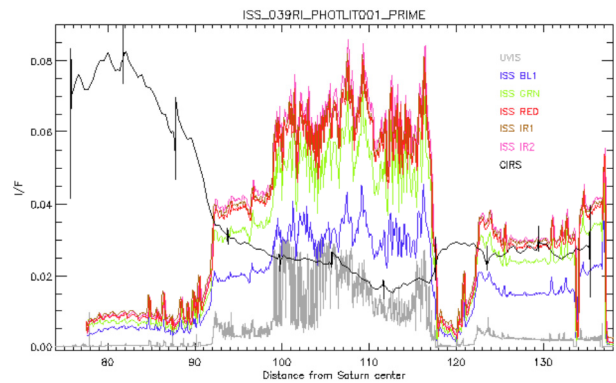
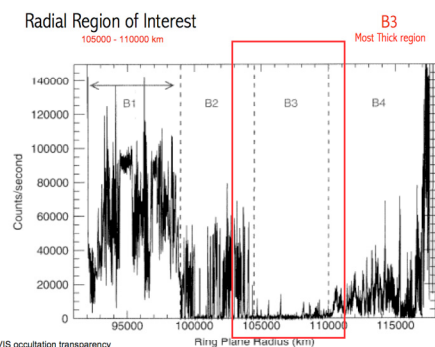


Figure 6. Radial Profiles

Radial Curves

Displayed in Figure 6 are radial curves (I/F versus saturnocentric distance) with respect to five of our six-working ISS filters (vio is here excluded) overplotted with a UVIS optical depth profile and a CIRS radial

Figure 7. B3 Occultation Transparency



curve for the observation ISS_039RI_PHOTLIT001_PRIME at a phase angle of 119.641°. Notice the color filters' radial dependence. Put differently, notice the separation in the blue and green filters, which is present in the B ring and not present in either the C or A rings. Also notice the IR1 and IR2 inversion with respect to the C and A rings.

B3 Region

After producing radial curves for all of the rings, we then focused on the optically thick, radial region of 105,000 – 110,000km of the B ring (Figure 7.)

Phase Curves

We first wished to examine the behavior of ISS optical (I/F) phase curves with CIRS thermal (T) phase curves.

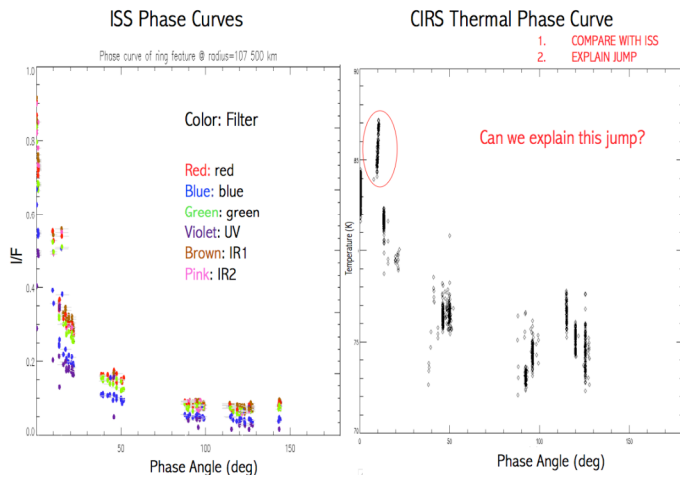


Figure 8. ISS I/F and CIRS T phase curves

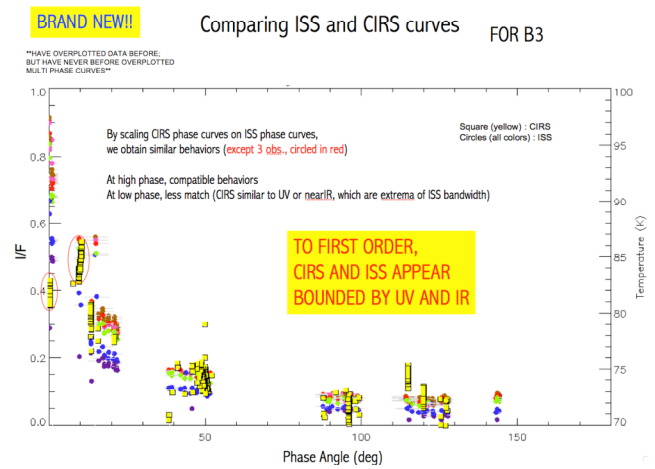
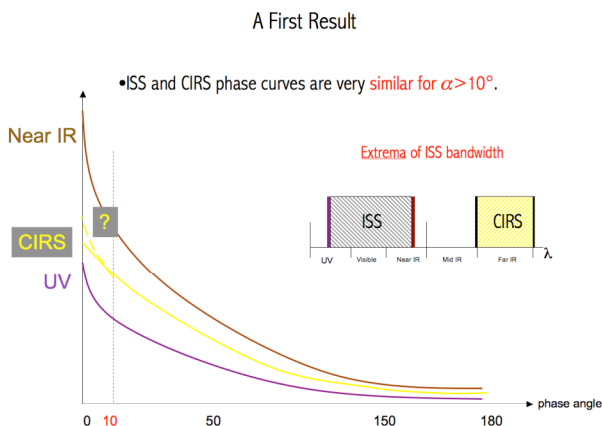


Figure 9. ISS and CIRS Phase Curve Comparison

Figure 8 displays optical and thermal phase curves. We immediately notice that high phase behavior appears compatible and that the thermal behavior appears both discontinuous (if both of the “jump” observations are maintained) and linear or non-linear (if one of the “jumping” observations is removed). We next overplotted I/F with Temperature to see in detail our original propositions (Figure 9). We notice that in our brand new as yet unexamined overplotting of CIRS with ISS phase curves, to first order, CIRS and ISS appear bounded below by the UV filter and above by the IR filters. That is, the CIRS curve falls somewhere in their between. Which leads to our first result that the CIRS curve is bounded by the extrema of the ISS bandwidth (Figure 10.)

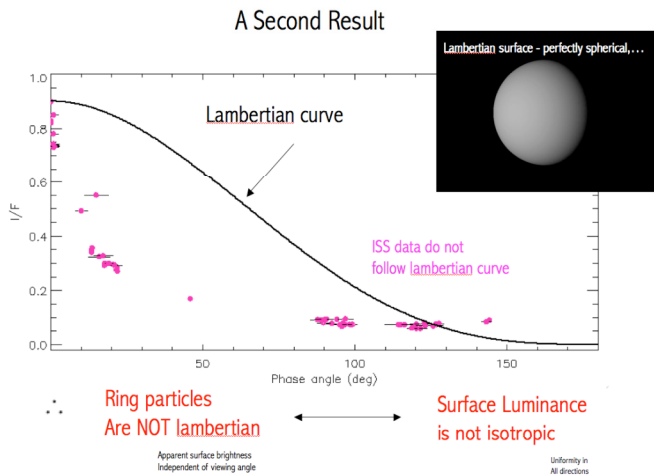
Figure 10. A First Result



A parenthetical interesting note:

We wished for lit images above 150° phase so as to track the high phase behavior to see whether it is slightly exponential (that is almost symmetrical with respect to y values) or whether it flattens out or remains absolutely invariant. After much image processing, we finally realized that we were geometrically constrained. That is, it was an impossibility to achieve lit images for a phase angle greater than 150° within our solar 12°-14° range. (Consult the appendix for the phase cone, which depicts this geometric constraint).

Figure 11. A Second Result



Secondly, we proposed and verified that as our ring particle phase behavior is not of the lambertian form, the ring particles are most likely not lambertian (Figure 11). Now, this is a point of controversy even though this is not a formal conclusion. In our ring models, we are forcing together discrete ring particulates and a homogenous conduction field into a “ring medium” which we model and thereby call a ring. Hence, what may be extracted from the phase curve is the nature of the regolith of the “rings” which can mean either the “ring particles” or the homogenous conduction media; therein rendering our conclusion not valid due to at minimum inconsistent premises. Still the behavior of either is not lambertian and hence the surface luminosity is anisotropic and apparent brightness is not independent of viewing angle.

We next tackled our second goal with respect to overplotting the optical and thermal phase curves (Figure 12). Removing one of the two jump observations lead to a drastically different CIRS phase curve behavior. Specifically, removal of the 0phase observation left a CIRS non-linear below 50° phase; while removal of the SUBML observation resulted in a linear CIRS behavior below 50° phase. Another puzzle is to determine which (if either) is the deviant observation, therein supporting or dismissing evidence of the thermal opposition effect in B3 (assuming there exists no error in data, plotting, etc...)

NOTICE TWO INTERPRETATIONS:

WHICH IS DEVIANT OBSERVATION?

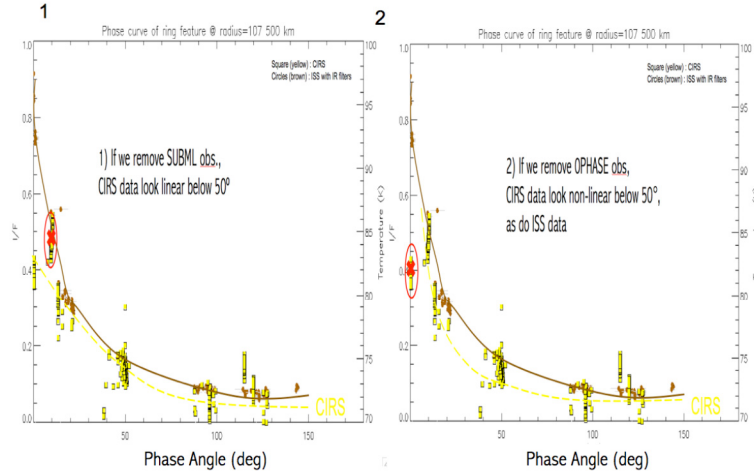


Figure 12. Two Interpretations

We next hypothesized explanations for this jump in the CIRS phase curve – two geometrical and one instrumental. Figure 13 displays temperature versus phase color coded with local time, spacecraft elevation angle, and footprint size, respectively. Simply, local time is particle time with respect to the sun. Spacecraft elevation is the angle between the spacecraft and the ring plane. And footprint is the spatial response of the CIRS instrument, which follows a two-dimensional Gaussian form and which in a sense reveals the tracks of CIRS in its radial and azimuthal scans of the rings.

Explanations?

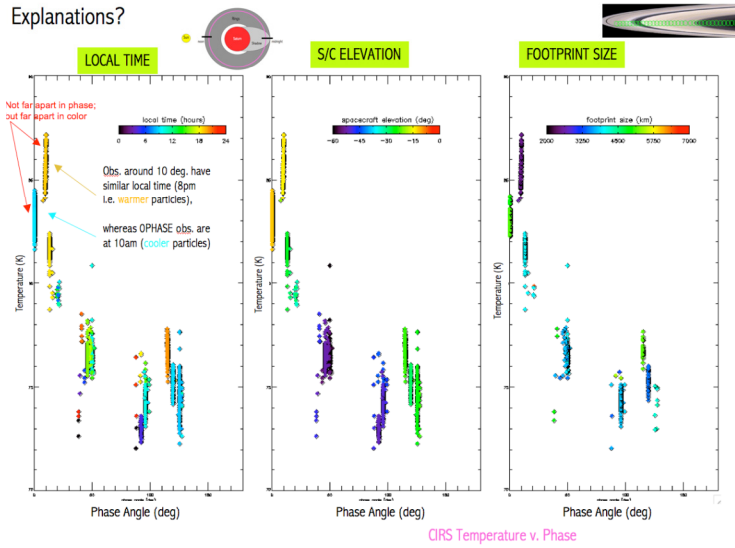


Figure 13. Proposed Explanations

We notice the following: There exists a color discontinuity in the local time frame. That is, while there exists a small difference in phase angles, there exists a large difference in local time. The surge in temperature can therefore be explained easily as ring particles left in the sun for a longer period of time will be warmer than those less exposed. Spacecraft elevation displays a rather continuous behavior with respect to the two jump observations and so can be ruled out as a factor, while footprint size again displays a jump in color for a relatively small difference in phase. Yet another puzzle is why

a smaller footprint at a solar elevation angle of 12°-14° at low phase would display a warmer temperature than that of a larger size footprint. We also considered, in Figure 15, the role of local volume density (that is the local filling factor) and examining the following plots, as we do not see the expected inverted behavior (as temperature and beta are inversely related) we can rule out beta as a factor. Again, these ruling outs are informal and worthy of a more thorough analysis, an analysis precluded by my fellowship tenure.

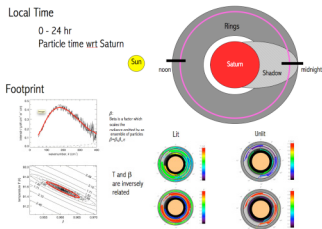


Figure 14. Explanation of Parameters

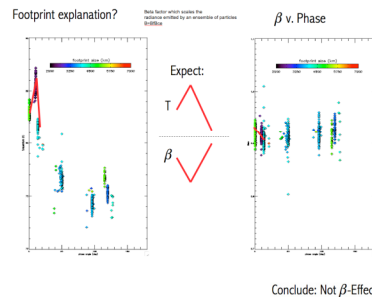
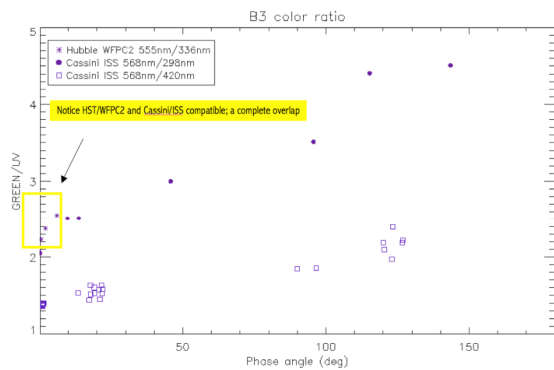


Figure 15. Not β Effect

Color Ratio

We next, in agreement with Cuzzi et. al, found an alternate way of comparing reflectivity profiles (I/F) across varying geometries: that of color ratios (Figure 16). Specifically, we created ratios of different filters for profiles obtained at the same geometries. To compare with Cuzzie et. al, who used ratios of Green/UV to investigate HST (Hubble Space Telescope) data sets obtained for the phase range of 0° to 6°, we took

Figure 16. B3 Color Ratio



Q: Why the spread in \square ?

Next Step:
Other Color Ratios &
Other Color Ratios in Other Regions

Green/(UV+UV3) and Green/VIO ratios with the following results: First, there exists a complete overlap/behavioral compatibility in HST/WFC2 and Cassini/ISS. That is, Cassini's ISS low phase points completely coincide with HST data points! Second, there is noticed a considerable spread in VIO data points; another puzzle awaiting devouring. Third, the color ratios increase with increasing phase angle and we therefore see reddening with increasing phase angle in the

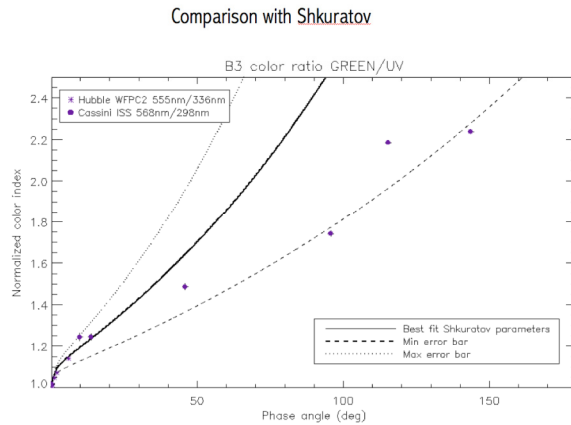


Figure 17. Normalized Color Ratio Comparison with Shkuratov

imply a role for “multiple scattering of some kind with increasing phase angle.” And secondly, determining the roles of multiple interparticle scattering, multiple scattering in the regolith, and multiple scattering between facets into on phase variation and on A and B ring color ratios and reflectivities. Regardless, the message here is in alignment with that of our introduction: the rings are a complex compositional machine with differing radial distributions whose nature is all but mechanics.

We next computed a normalized color ratio to compare our work with that of the Shkuratov model (Figure 17) and found that our B3 color ratios (Green/UV for HST WFPC2 and Cassini ISS) were best fit by the extrema of the model’s parametric error bars. Specifically, “k”, the roughness parameter, was the most sensitive parameter whose selective varying produced the nice fit; that is, the sufficiency for a good fit being a combination of k min and k max. This shows the overall robustness of Shkuratov’s model in the ability of its fitting function to extrapolate from a 0° to 6° to a 0° to 180° phase range, therein fitting the high phase data, a task quite impressive.

B3 Spectra

My fellowship concluded with the following: Figure 18 reveals (for the B3 region) HST spectra at 6° phase overplotted with ISS spectra at four phase increments of 0.9°, 23°, 45°, and 123° (working in units of I/F (1/str) versus wavelength (nm) and found the following: one, I/F increases with increasing wavelength and secondly, the shape flattens out with increasing phase. A puzzle is whether the ‘F’ factor in I/F (the phase-corrected reflectivity correction) accounts for solar cycles along with accounting for the distance to the sun (private correspondence, Scott Edgington).

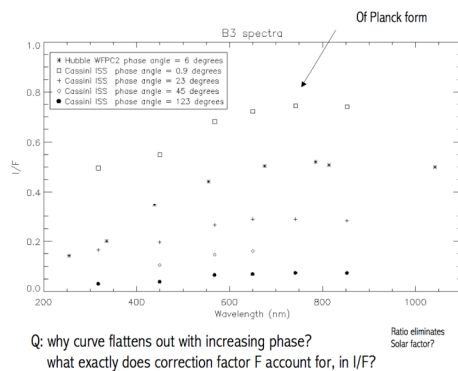


Figure 18. B3 Spectra

Figure 19 reveals a B3 spectra (Intensity versus wavelength in microns) of ISS and CIRS at 0.9° overplotted with a Solar Spectrum and an Earth-based Saturn and Saturn’s rings’ spectrum, (where the ISS spectra have been roughly “ratioed” into intensity units and the CIRS “tail” extension is phenomenal as CIRS is invalid beyond 1000 microns). (We note parenthetically that obtaining the solar spectra in the correct units was not straight forward; with the help of Bob West we successfully converted from photons per angstrom to Watts per micron (Figure 20); we thank you Bob West).

336 – 555nm spectral range, in complete agreement with Cuzzi et. al. Once we extend our work to other B ring regions we can investigate the alleged correlation between optical depth and color and the lack of correlation between ring reflectivity and color in the B ring. To double check Cuzzi’s concluding propositions, we will need to explain two things: the correlated varying ring reflectivity and phase angle variation in certain wavelength regions which may indicate that the varying color ratio is not a “particle-size dependent effect” and which, as the redness of red regions increases with phase angle, may

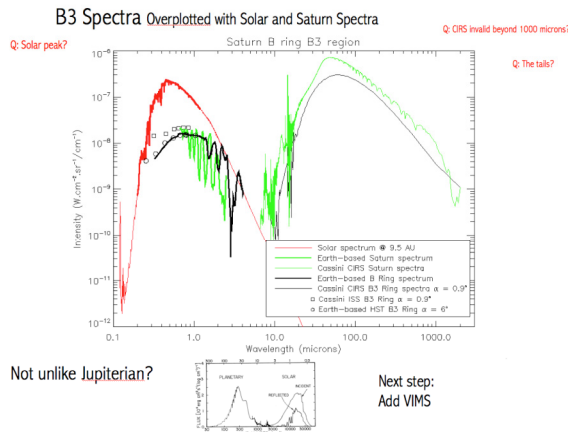


Figure 19. Overplotted Spectra

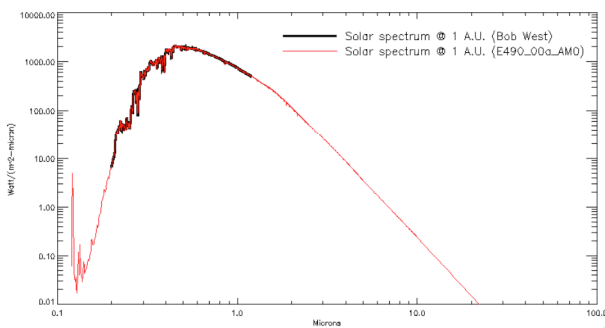


Figure 20. Solar Spectrum Fit From Bob West

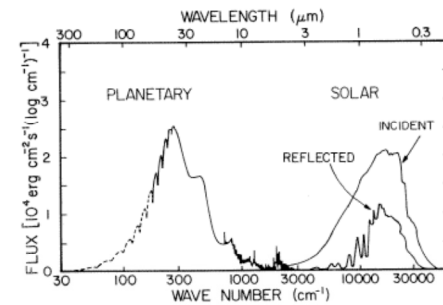


Figure 21. Flux Comparison

We speculated that the signal to noise ratio increases with phase as evinced in the displayed FP1 and FP3 noise and, by comparing Jovian spectra (Figure 21), that the Saturnian spectra are both quite different from the Jovian, with emitted light never peaking beyond solar, but are also quite similar in the crossing of solar with emitted light and solar eclipsing reflected light. We are in the process of overplotting VIMS spectra and once UVIS is overplotted, we will have obtained again a new result featuring co-registered multi-plotted spectra from all 4 remote optical sensing devices!

Discussion

We have produced at different wavelengths thermal and optical phase curves for selected locations in the rings, thereby compiling the many independent results of the rings from ISS, VIMS, and CIRS data sets. We see there exist wavelength dependent features.

Conclusions:

First and most important, ISS and CIRS phase curves have been overplotted for the first time! We note that data sets have before been overplotted, but not phase curves. Secondly, we note that in order to conclude whether the CIRS behavior below 50° phase is non-linear or linear we clearly need new data in the 0° to 10° phase region; that is, we need better phase sampling range. Third and fourth we show that the CIRS behavior is bounded by ISS bandwidth extrema and that the ring particles do not follow a lambertian behavior. Fifth we have shown HST, ISS, and CIRS commensurability and Shkuratov’s extrapolation to high phase. Finally, the most exciting are the three resultant puzzles of low-phase behavior, similarity in analytical extrapolation to other ring regions, and the meaning of the overlapping spectra.

Future Work:

The next step in the research plan (part two of the proposal) is to derive a well constrained albedo in distinction to both Dones and Morishima. Our approach will be novel in both covering all phase space and being independent of the coupled model input parameters; that is, bond albedo will no longer be a free variable. We originally sought out adding-doubling code for this derivation but did not succeed as we could find no model suited to our complex parameter space requiring covering all of phase space. Hence we will use our novel and complex idea using shadow functions, N-body, and ray tracing code. Secondly, what is still relatively unexplored, as we have reproduced the flatness of the B3 ring unlit thermal phase curves, they and the concomitant local time curves will need further examination.

Thirdly, what is still beyond our grasp is the visible opposition effect (VOE) observed by Muller (1883) at optical wavelengths; specifically the mechanistic coupling of inter/intra-particle shadow hiding and coherent backscattering. Perhaps our knowledge of the thermal opposition effect (observed by Altobelli (2007) in far-infrared) will aid in understanding the visible opposition effect as the TOE is most plausibly independent of the coherent backscattering. The present work's compilation of multi-wavelength data sets still does not contain enough information toward complete VOE and TOE understanding. Per Deau's investigation, only upon acquisition of more multi-wavelength data can we comprehend the relation between the broad thermal surge and the narrow visible opposition surge.

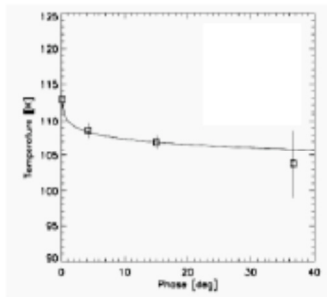


Figure 22. TOE Effect

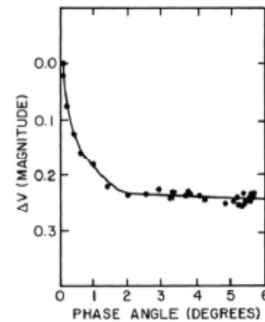


Figure 23. VOE Effect

Acknowledgments

My gratitude to the CIRS team is of ordinal order. I give to Dr.s Spilker and Deau for their omni-guidance and non-captious advisement, my most respectful thank you. The opportunity to work for this singular omni-international team of thinkers is immeasurably appreciated. Thank you National Aeronautical and Space Administration and SURF for sponsoring my fellowship of creation/learning.

References

- Altobelli, N., L. Spilker, S. Pilorz, S. Brooks, S. Edgington, B. Wallis, M. Flasar, 2007. C ring fine structures revealed in the thermal infrared, *Icarus*, 191, 691–701.
- Altobelli, N., L. J. Spilker, C. Leyrat, S. Pilorz, 2008. Thermal observations of Saturn's main rings by Cassini CIRS: Phase, emission and solar elevation dependence, *Planetary and Space Science*, 56, 134–146.
- Cuzzi, J., Lissauer, J., Esposito, L., Holberg, J., Marouf, E., Tyler, G., Boischot, A., 1984. Saturn's rings: properties and processes. In: Greenberg, R., Brahic, A. (Eds.), *Planetary Rings*. University of Arizona Press, pp. 73–199.
- Flasar, F.M., ... L.J. Spilker, and Cassini CIRS team. 2004. Exploring the Saturn System in the thermal infrared: The Composite Infrared Spectrometer. *Space Science Rev.*, Vol. 114, Nos. 1-4, Kluwer Academic Publishers, 169-297.
- Leyrat C., Ferrari C., Charnoz S., Decriem J., Spilker L. J., Pilorz S. H., Spinning particles in Saturn's C ring: Pre-Cassini results, 2008a, *Icarus*, Volume 196, Issue 2, p. 625-641.
- Leyrat, C., L. J. Spilker, N. Altobelli, S. Pilorz, C. Ferrari, 2008b. Infrared observations of Saturn's rings by Cassini CIRS : Phase angle and local time dependence, *Planetary and Space Science*, 56, 117–133.
- Morishima, R, et al. (2009a). A Multilayer model for thermal infrared emission of Saturn's rings: Basic formulation and implications for Earth-based observations. *Icarus*, 201, 634-654.

Morishima, R, et al. (2009b). A Multilayer model for thermal infrared emission of Saturn's rings II: Particle properties estimated from Cassini-CIRS data in the early phase. Submitted to *Icarus* (June 2009) Revised June 2010.

Stuart J. Robbins, Glen R. Stewart, Mark C. Lewis, Joshua E. Colwell, Miodrag Sremcevic. Estimating the Masses of Saturn's A and B Rings from High-Optical Depth N-Body Simulations and Stellar Occultations, *Icarus*, 206 (2010) 431-445.

H. Salo and R. Karjalainen. Photometric Modeling of Saturn's Rings. I. Monte Carlo Method and the Effect of Nonzero Volume Filling Factor. *Icarus*, 164 (2003) 428-460.

H. Salo, R. Karjalainen, and R. G. French. Photometric Modeling of Saturn's Rings. II. Azimuthal Asymmetry in Reflected and Transmitted Light. *Icarus*, 170, (2004) 70-90.

Spilker, L. J., S. H. Pilorz, B. D. Wallis, J. C. Pearl, J. N. Cuzzi, S. M. Brooks, N. Altobelli, S. G. Edgington, M. Showalter, F. M. Flasar, C. Ferrari, C. Leyrat, 2006. Cassini Thermal Observations of Saturn's main rings: Implications for particle rotation and vertical mixing, *Planetary and Space Science*, 54, Issue 12, 1167-1176.

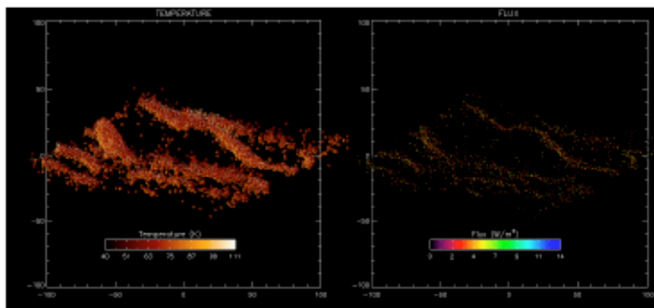
Spilker, L., S. Pilorz, B. Wallis, S. Edgington, S. Brooks, J. Pearl, J., F. Flasar, 2005. Cassini CIRS Observations of a Roll-off in Saturn Ring Spectra at Submillimeter Wavelengths. *Earth, Moon and Planets*, Volume 96, Issue 3-4, 149-163.

Appendix

Ring Modeling

Ring structure is most likely a monolayer for the largest particles, while a multilayer can characterize the vertically extended small particles. And where there exist self-gravity wakes or viscous overstability, there does not exist ring uniformity. Attempts to model such a non-trivial structure are optical and thermal monolayer and multilayer models, as well as ray tracing applied to output of N-body simulations for optical light. What complicates thermal modeling is that thermal energy is transported by particle's spin and translational motion in addition to radiation. So our thermal models must follow the time evolution of thermal emission coupled with N-body simulations.

Figure 24. N-Body Simulation and Ring Particle Wakes



quantified in a bimodal size distribution; and the heat transport due to particles' motion in the vertical azimuthal directions is considered.

The model with which data was fit is a dynamical, thermal model constructed by Co_I Morishima. It is a multilayer model in which: the equation of classical radiative transfer is solved for both visible and infrared light adopting, without wakes, a plane-parallel approximation; the vertical heterogeneity of spin frequencies of ring particles is considered and

We note, parenthetically, that the multilayer model used included neither regolith for individual ring particles or wakes nor representation of particle compaction. Per Lagerros, we will need to consider surfaces craters and planar facets, parameterized by the fraction of craters in a unit section and the maximum slope of a crater; and to consider thermal beaming (a non-Lambertian reflection) and modeling

the ring particles as stochastic surfaces (meaning in effect there exists some indeterminacy in the future behavior of the ring particle independent of its initial conditions). We clearly need a realistic distribution of ring particles, along the lines of Lagerros meets advanced ray tracing.

Phase Cone

The phase cone displays, for a designated value of solar elevation, spacecraft elevation versus phase angle. What is important is to note that one can now easily determine the possible range of spacecraft elevations for specified solar and phase values. Also apparent is that the values of longitude and spacecraft are immutably constrained by the solar elevation and phase values, which precludes in advance any impossible non-sensical geometries.

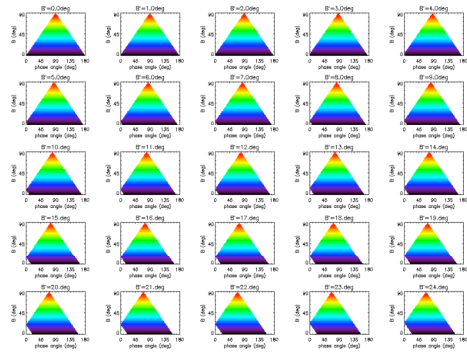


Figure 25. The Phase Cone – A Geometric Constraint